

Towards ISAC RIS-Enabled Passive Radar Target Localization

Ahmad Bazzi*[†] and Marwa Chafii*[†]

*Engineering Division, New York University (NYU), Abu Dhabi, UAE.

[†]NYU WIRELESS, NYU Tandon School of Engineering, New York, USA

Abstract—Incorporating integrated sensing and communication capabilities into forthcoming 6G wireless networks is crucial for achieving seamless synchronization between the digital and physical worlds. The following paper focuses on a scenario where a passive radar (PR) is subject to weak line-of-sight signals of opportunity, emanating from an access point and subsequently reflecting off targets, ultimately reaching the PR. Furthermore, a normalized least mean squares method is presented for jointly detecting the number of targets and estimating target angles of arrival (AoAs). The algorithm iteratively adjusts the steering vector estimates to minimize a suitable error cost function, while the target AoAs are identified via a peak-finding search conducted on the resulted power spectrum. Simulation results show the capabilities of the proposed localization method, as well as a 14 dB dynamic range reduction that can be achieved at the PR.

Index Terms—integrated sensing and communications (ISAC), passive radar (PR), target localization, dynamic range (DR), reconfigurable intelligent surface (RIS)

I. INTRODUCTION

Research on 6G envisions future services and applications, targeting diverse market demands and disruptive technologies. 6G aims to support an array of services like blockchain, haptic telemedicine, VR/AR remote services, holographic teleportation, and extended reality (XR). It goes beyond mere connectivity, integrating sensing, computing, and utilizing environmental data for AI and machine learning. Nevertheless, bandwidth-demanding applications necessitate a significant capacity increase, expected to rise by a factor of 10^3 by 2030. Enabling technologies like sub-6 GHz, milli-meter wave (mmWave) frequencies, and reconfigurable intelligent surface (RIS) play crucial roles.

RISs, composed of reconfigurable reflecting elements, have garnered attention for their capability to enhance wireless sensor networks’ capacity and coverage [1]. These structures manipulate incident signals in the wireless propagation environment, altering wireless channels between network nodes. RISs offer low energy consumption, allowing signal amplification without power amplifiers. Yet, their low cost might lead to large-scale deployment, sprawling entire building walls [2]. Properly designed phase shifts from each reflecting element combine reflected signals effectively. They are known as large intelligent surface/antennas (LISA) or intelligent reflecting surface (IRS) in literature. RISs have diverse applications in wireless communications, such as beamforming, security, OFDM, and millimeter-wave channel estimation [3]–[5]. Their deployment enhances spectral and energy efficiency, aids in

environment-friendly deployment, and offers secure wireless communication [6], [7]. Over the last 80 years, passive radar, which localizes targets without emitting controlled radar data, has been extensively studied [8], [9]. RIS is anticipated to be pivotal in advanced localization and sensing [10] applications via passive radar. Passive radar offers cost-effective procurement, operation, and maintenance, as well as covert operation. However, it faces challenges in target localization due to the absence of transmit waveform information. Nonetheless, it is protocol-agnostic and lacks active component assistance in some instances.

Channel estimation, typically between any two nodes within the system, is essential for designing the reflective matrix, which involves phase shifters at the RIS. One approach, as in [11], employs deep learning and compressive sensing techniques for RIS phase shift design without requiring channel estimation for target localization. An alternative approach in [12] suggests an adaptive RIS phase shifter using hierarchical codebooks with UE feedback for localization, yet it differs fundamentally from our scenario. Specifically, it doesn’t involve passive radar (PR) or leverage multipath bounces off targets for localization. Similarly, works such as [13] and [14] perform localization with RIS but without PR, where the latter also lacks reflections from the targets. In contrast to these approaches, our proposed model involves PR performing spatial beamforming towards the RIS, focusing on reflections bouncing off the targets towards the RIS, which redirects these bounces towards the PR. Conversely, works such as [15] optimize RIS phase shift coefficients using received signal strength (RSS) values to maximize location change differences.

The focus of this paper is on a situation where a PR is exposed to weak line of sight (LoS) signals of opportunity created by communication signals transmitted by an access point (AP), and further reflected off targets, ultimately reaching the PR. Indeed, PR can suffer from short operational range and low range resolution problems [16], in addition to distant targets, which tend to have obstructed or very weak LoS signal [17]. To address this, a RIS is deployed to cover the entire environment, establishing robust LoS connections with both the targets and the PR. To this end, the contributions of the paper can be summarized as follows: We formulate an appropriate system model to represent the aforementioned situation. Due to the power discrepancies within the received signal, the RIS modifies its phase shifts in coordination with

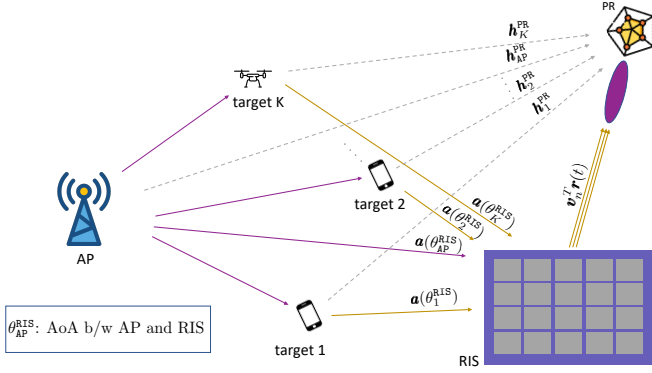


Fig. 1. The scenario involves an RIS-based multi-target system, where an AP serves communication users in the downlink. The system includes an RIS with M elements, which reflects signals bouncing off targets towards the PR. **The dashed lines model weak LoS components, whereas the solid lines model a strong LoS channel.**

PR beamforming, ensuring the robust reception of the LoS signals for further localization, while minimizing the required dynamic range (DR) at the PR. Furthermore, an adaptive approach based on normalized least mean squares (NLMS) is introduced, aiming to concurrently discern the number of targets and estimate their respective angle of arrivals (AoAs). Through iterative refinement of the steering vector estimates, the algorithm minimizes a suitable error cost function, while the target AoAs are identified via a peak-finding search conducted on the resulted power spectrum. The simulation results demonstrate the efficacy of the proposed localization method and reveal a notable 14 dB reduction in DR achievable at the PR.

The following paper is organized as follows: Section II introduces the system model of the underlying problem. Section III optimizes the RIS phase shifts as well as the PR beamforming weights to achieve a low DR at the PR. Section IV, we describe a technique for simultaneously detecting the number of targets and estimating target AoAs. Section V presents our simulation results.

Notation: Upper-case and lower-case boldface letters denote matrices and vectors, respectively. $(\cdot)^T$, $(\cdot)^*$ and $(\cdot)^H$ represent the transpose, the conjugate and the transpose-conjugate operators. The statistical expectation is denoted as $\mathbb{E}\{\cdot\}$. For any complex number $z \in \mathbb{C}$, the magnitude is denoted as $|z|$, its angle is $\angle z$. The ℓ_2 norm of a vector \mathbf{x} is denoted as $\|\mathbf{x}\|$. The matrix \mathbf{I}_N is the identity matrix of size $N \times N$. The zero-vector is $\mathbf{0}$. For matrix indexing, the $(i, j)^{th}$ entry of matrix \mathbf{A} is denoted by $\mathbf{A}_{i,j}$. The sub-matrix of \mathbf{A} ranging from rows i_1 to $i_2 > i_1$ and columns j_1 to $j_2 > j_1$ is denoted as $\mathbf{A}_{i_1:i_2, j_1:j_2}$.

II. SYSTEM MODEL

Let's consider a scenario involving a narrow-band system tasked with localizing K targets. In this context, communication users are also considered targets. To simplify, consider a single-antenna AP transmitting a signal, denoted as $s(t)$. In an integrated sensing and communications (ISAC) framework, the signal $s(t)$ initially intended for communication purposes,

is also exploited by the radar sub-systems [18], specifically the PR. In the deep learning (DL) transmission, the AP broadcasts $s(t)$ through an omni-directional antenna. Consequently, the signal reaches and bounces off the K targets, whereby the RIS receives those reflections, along with the direct signal path between the AP and RIS itself. As a result, the signal received at the RIS can be described as

$$\mathbf{r}(t) = \mathbf{A}(\Theta_{1:K}^{\text{RIS}})\mathbf{s}(t) + \alpha_0 \mathbf{a}_M(\theta_{\text{AP}}^{\text{RIS}})s(t - \tau_{\text{AP}}^{\text{RIS}}), \quad (1)$$

where the LoS element is denoted by $\mathbf{a}_M(\theta_{\text{AP}}^{\text{RIS}})$, where $\theta_{\text{AP}}^{\text{RIS}}$ signifies the angle between the RIS and the k^{th} target. In fact, the complex vector $\mathbf{a}_M(\theta) \in \mathbb{C}^{M \times 1}$ denotes the input array steering vector for the RIS toward an AoA θ , which is represented as

$$\mathbf{a}_M(\theta) = [a_1(\theta) \quad \dots \quad a_M(\theta)]^T. \quad (2)$$

Likewise, $\mathbf{a}_M(\theta_{\text{AP}}^{\text{RIS}})$ is the LoS component between AP and RIS, $\theta_{\text{AP}}^{\text{RIS}}$ is the AoA between AP and RIS, and $\mathbf{h}_{\text{AP}}^{\text{RIS}}$ is the non-LoS component between AP and RIS. In addition, $\kappa_{\text{AP}}^{\text{RIS}}$ is the Rician factor for the channel between AP and RIS. In addition, $\mathbf{A}(\Theta_{1:K}^{\text{RIS}})$ is the steering matrix, deriving from the combined contribution of each path between the targets and the RIS, which is given as $\mathbf{A}(\Theta_{1:K}^{\text{RIS}}) = [\mathbf{a}_M(\theta_1^{\text{RIS}}) \quad \mathbf{a}_M(\theta_2^{\text{RIS}}) \quad \dots \quad \mathbf{a}_M(\theta_K^{\text{RIS}})]$. Here, the steering vector $\mathbf{a}_M(\theta) \in \mathbb{C}^{M \times 1}$, characterizes the steering at the output of the M elements within the RIS. The signal $\mathbf{s}(t) \in \mathbb{C}^{K \times 1}$ contains scaled and delayed versions of the original transmitted signal $s(t)$, where its k^{th} entry is given as $[\mathbf{s}(t)]_k = \alpha_k s(t - \tau_{\text{AP}}^k - \tau_k^{\text{RIS}})$, where the following parameters encapsulate the propagation delays within the system, i.e. τ_{AP}^k is the delay between the AP and the k^{th} target, τ_k^{RIS} is the delay between the k^{th} target and the RIS, and $\tau_{\text{AP}}^{\text{RIS}}$ is the delay the AP and the RIS. Moreover, α_k represents the reflection gain, encompassing large-scale fading effects of the two-way AP-target-RIS. However, α_0 serves as a complex coefficient considering the direct channel gain specifically between the AP and the RIS. To this end, the expression describing the signal reflected by the RIS towards the PR is presented as

$$x_n(t) = \mathbf{b}_M^T(\phi_{\text{RIS}}^{\text{PR}})\Theta^{(n)}\left(\mathbf{A}(\Theta_{1:K}^{\text{RIS}})\mathbf{s}(t) + \alpha_0 \mathbf{a}_M(\theta_{\text{AP}}^{\text{RIS}})s(t - \tau_{\text{AP}}^{\text{RIS}})\right). \quad (3)$$

Here, $\Theta^{(n)} = \text{diag}(e^{j\beta_1^{(n)}}, e^{j\beta_2^{(n)}} \dots e^{j\beta_M^{(n)}})$ represents the RIS shifting elements during the n^{th} epoch. An epoch signifies a time period where a realization of $\mathbf{r}(t)$, as defined in equation (1), is received. Therefore, $\beta_m^{(n)}$ specifically denotes the phase shift at the m^{th} RIS element during the epoch n . The vector $\mathbf{b}_M(\phi) \in \mathbb{C}^{M \times 1}$ defines the output transmit steering vector of the RIS, articulated as $\mathbf{b}_M(\phi) = [b_1(\phi) \quad \dots \quad b_M(\phi)]$. The angle $\phi_{\text{RIS}}^{\text{PR}}$ represents the angle of departure (AoD) from the RIS to the PR. Particularly, in the scenario assuming a LoS channel between the RIS and the PR, the channel between each RIS element and the PR is denoted by $\mathbf{b}_M^T(\phi_{\text{RIS}}^{\text{PR}})$. Finally, the signal received at the PR can be represented as

$$\mathbf{y}_n(t) = \rho_{\text{RIS}}^{\text{PR}} \mathbf{a}(\theta_{\text{RIS}}^{\text{PR}})x_n(t - \tau_{\text{RIS}}^{\text{PR}}) + \rho_{\text{AP}}^{\text{PR}} \mathbf{h}_{\text{AP}}^{\text{PR}} s(t - \tau_{\text{AP}}^{\text{PR}}) + \sum_{k=1}^K \rho_k \mathbf{h}_k^{\text{PR}} s(t - \tau_{\text{AP}}^k - \tau_k^{\text{PR}}) + \epsilon_n(t). \quad (4)$$

The channel $\mathbf{h}_{\text{AP}}^{\text{PR}}$ is described as a combination of the LoS component, denoted by $\sqrt{\frac{\kappa_{\text{AP}}^{\text{PR}}}{1+\kappa_{\text{AP}}^{\text{PR}}}} \mathbf{a}(\theta_{\text{AP}}^{\text{PR}})$, and the non-LoS component $\sqrt{\frac{1}{1+\kappa_{\text{AP}}^{\text{PR}}}} \bar{\mathbf{h}}_{\text{AP}}^{\text{PR}}$, namely

$$\mathbf{h}_{\text{AP}}^{\text{PR}} = \sqrt{\frac{\kappa_{\text{AP}}^{\text{PR}}}{1+\kappa_{\text{AP}}^{\text{PR}}}} \mathbf{a}(\theta_{\text{AP}}^{\text{PR}}) + \sqrt{\frac{1}{1+\kappa_{\text{AP}}^{\text{PR}}}} \bar{\mathbf{h}}_{\text{AP}}^{\text{PR}}. \quad (5)$$

Here, $\kappa_{\text{AP}}^{\text{PR}}$ characterizes the Rician factor representing the channel between the AP and the PR, while $\bar{\mathbf{h}}_{\text{AP}}^{\text{PR}}$ refers to the non-LoS part of that channel. Similarly, the expression for \mathbf{h}_k^{PR} encompasses the Rician factor κ_k^{PR} for the k^{th} target and the PR. It involves the LoS component $\sqrt{\frac{\kappa_k^{\text{PR}}}{1+\kappa_k^{\text{PR}}}} \mathbf{a}(\theta_k^{\text{PR}})$ and the non-LoS component $\sqrt{\frac{1}{1+\kappa_k^{\text{PR}}}} \bar{\mathbf{h}}_k^{\text{PR}}$, representing the non-LoS link between the k^{th} target and the PR, i.e.

$$\mathbf{h}_k^{\text{PR}} = \sqrt{\frac{\kappa_k^{\text{PR}}}{1+\kappa_k^{\text{PR}}}} \mathbf{a}(\theta_k^{\text{PR}}) + \sqrt{\frac{1}{1+\kappa_k^{\text{PR}}}} \bar{\mathbf{h}}_k^{\text{PR}}. \quad (6)$$

In equation (4), the vector $\mathbf{y}_n(t) \in \mathbb{C}^{N_{\text{PR}} \times 1}$ signifies the received signal at the PR. Summarizing the system model as illustrated in Fig. 1, the terms within the equation represent different aspects, which are the following; the first term, $\rho_{\text{RIS}}^{\text{PR}} \mathbf{a}(\theta_{\text{RIS}}^{\text{PR}}) x_n(t - \tau_{\text{RIS}}^{\text{PR}})$, capsulizes all the sensing data collected at the RIS and reflected back to the PR. The second term, $\rho_{\text{AP}}^{\text{PR}} \mathbf{h}_{\text{AP}}^{\text{PR}} s(t - \tau_{\text{AP}}^{\text{PR}})$, represents the channel between the AP and the PR. The third term, $\sum_{k=1}^K \rho_k \mathbf{h}_k^{\text{PR}} s(t - \tau_{\text{AP}}^k - \tau_k^{\text{PR}})$, involves the contributions from the K targets. These signals propagate from the AP to the targets and then bounce back towards the PR. Here, $\tau_{\text{RIS}}^{\text{PR}}$ refers to the delay between the RIS and the PR, $\tau_{\text{AP}}^{\text{PR}}$ is the delay between the AP and the PR, and τ_k^{PR} signifies the delay between the k^{th} target and the PR. Moreover, the large-scale fading gains, represented by ρ_k , are defined in a similar manner as the α_k s. Furthermore, the term $\epsilon_n(t)$ represents the noise, particularly additive white Gaussian noise (AWGN). Sampling equation (4) at L time instances and concatenating the samples provides

$$\begin{aligned} \mathbf{Y}_n &= [\mathbf{y}_n(t_1) \quad \mathbf{y}_n(t_2) \quad \dots \quad \mathbf{y}_n(t_L)] \\ &= \rho_{\text{RIS}}^{\text{PR}} \mathbf{a}(\theta_{\text{RIS}}^{\text{PR}}) \mathbf{x}_n + \rho_{\text{AP}}^{\text{PR}} \mathbf{h}_{\text{AP}}^{\text{PR}} \mathbf{s}_{\text{AP}}^{\text{PR}} + \sum_{k=1}^K \rho_k \mathbf{h}_k^{\text{PR}} \mathbf{s}_k^{\text{PR}} + \mathbf{E}_n. \end{aligned} \quad (7)$$

Equation (7) defines the matrix $\mathbf{Y}_n \in \mathbb{C}^{N_{\text{PR}} \times L}$ as the collected sampled data matrix at the PR for the epoch n . In addition, the terms appearing in (7) are defined as

$$\mathbf{x}_n = [x_n(t_1) \quad x_n(t_2) \quad \dots \quad x_n(t_L)], \quad (8)$$

$$\mathbf{s}_{\text{AP}}^{\text{PR}} = [s(t_1 - \tau_{\text{AP}}^{\text{PR}}) \quad s(t_2 - \tau_{\text{AP}}^{\text{PR}}) \quad \dots \quad s(t_L - \tau_{\text{AP}}^{\text{PR}})], \quad (9)$$

$$\mathbf{s}_k^{\text{PR}} = \begin{bmatrix} s(t_1 - \tau_{\text{AP}}^k - \tau_k^{\text{PR}}) \\ s(t_2 - \tau_{\text{AP}}^k - \tau_k^{\text{PR}}) \\ \vdots \\ s(t_L - \tau_{\text{AP}}^k - \tau_k^{\text{PR}}) \end{bmatrix}^T, \quad (10)$$

$$\mathbf{E}_n = [\epsilon_n(t_1) \quad \epsilon_n(t_2) \quad \dots \quad \epsilon_n(t_L)]^T. \quad (11)$$

Collecting all samples at different epochs in one data matrix, we now have the following at the PR,

$$\mathbf{Y} = [\mathbf{Y}_1^T \quad \mathbf{Y}_2^T \quad \dots \quad \mathbf{Y}_{N_{\text{epoch}}}^T]^T \in \mathbb{C}^{N_{\text{PR}} N_{\text{epoch}} \times L}. \quad (12)$$

III. RIS AND PR OPTIMIZATION

In this section, we describe how the RIS the phase shifts to re-direct useful signals for localization towards the PR. In turn, we also describe how the PR can optimize its analog beamformer to receive the RIS signals with minimal interference. For the RIS, we propose the following

$$(\mathcal{P}_{\text{RIS}}) : \begin{cases} \min_{\beta_m^{(n)}} & \|\mathbf{b}_M^T(\phi_{\text{RIS}}^{\text{PR}}) \Theta^{(n)} \mathbf{a}_M(\theta_{\text{AP}}^{\text{RIS}})\|^2 \\ \text{s.t.} & \beta_m^{(n)} \in [-\pi, \pi], \quad \forall m \end{cases} \quad (13)$$

The RIS phase-shifter matrix is employed to *minimize the known contribution, i.e. AP-RIS-PR (experiencing double path-loss), which is a fixed path with considerably higher power compared to other paths, such as the AP-target-RIS-PR (experiencing triple path-loss) path*. This entails that an unnecessarily high DR would be needed at the PR to discern the smaller paths arising from AP-target-RIS-PR. The optimization problem presented in (14) aims to reduce the channel contribution between the AP and the RIS, rather than forming beams towards specific regions. The equivalent optimization problem (\mathcal{P}_{RIS}) can be expressed as follows

$$(\mathcal{P}_{\text{RIS}}) : \begin{cases} \min_{\mathbf{v}_n} & \|\mathbf{v}_n^T \tilde{\mathbf{a}}_M(\theta_{\text{AP}}^{\text{RIS}})\|^2 \\ \text{s.t.} & |[\mathbf{v}_n]_m| = 1, \quad \forall m, \end{cases} \quad (14)$$

where $\tilde{\mathbf{a}}_M(\theta_{\text{AP}}^{\text{RIS}}) = \mathbf{B} \mathbf{a}_M(\theta_{\text{AP}}^{\text{RIS}})$ and $\mathbf{B} = \text{diag}[\mathbf{b}_M(\phi_{\text{RIS}}^{\text{PR}})]$. Note that $[\mathbf{v}_n]_m = e^{j\beta_m^{(n)}}$, thanks to the constant modulus constraint. In addition, this optimization problem acts on an instantaneous basis, i.e. it computes the RIS phase shift coefficients, i.e. $\beta_m^{(n)}$ (equivalently $[\mathbf{v}_n]_m$) at epoch n . To optimize over the available epochs, the following optimization problem is proposed

$$(\mathcal{P}_{\text{RIS}}) : \begin{cases} \min_{\mathbf{V}} & \|\mathbf{V} \tilde{\mathbf{a}}_M(\theta_{\text{AP}}^{\text{RIS}})\|^2 \\ \text{s.t.} & |[\mathbf{V}_{n,m}]| = 1, \quad \forall n, m. \end{cases} \quad (15)$$

In equation (15), the matrix $\mathbf{V} = [\mathbf{v}_1 \quad \mathbf{v}_2 \quad \dots \quad \mathbf{v}_{N_{\text{epoch}}}]^T \in \mathbb{C}^{N_{\text{epoch}} \times M}$ concatenates all the phase-shift vectors. To this end, the optimization problem (\mathcal{P}_{RIS}) is non-convex due to the constant-modulus constraint. For this purpose, we suggest to: 1) solve the unconstrained optimization problem, then 2) adapt the solution towards a feasible one. Towards this goal, the unconstrained version of problem (\mathcal{P}_{RIS}) admits as solution,

$$\bar{\mathbf{V}} = \mathcal{P}_{\tilde{\mathbf{a}}_M(\theta_{\text{AP}}^{\text{RIS}})}^\perp = \mathbf{I}_M - \|\tilde{\mathbf{a}}_M(\theta_{\text{AP}}^{\text{RIS}})\|^2 \tilde{\mathbf{a}}_M(\theta_{\text{AP}}^{\text{RIS}}) \tilde{\mathbf{a}}_M^H(\theta_{\text{AP}}^{\text{RIS}}). \quad (16)$$

The above matrix requires a one-time computation. Furthermore, the solution is in-feasible, as there is no warranty on $\bar{\mathbf{V}}_{i,j}$ to satisfy the constant modulus constraint. In order to project onto the feasible set, the following solution is proposed

$$\mathbf{V} = \exp \left\{ j \angle (\mathcal{P}_{\tilde{\mathbf{a}}_M(\theta_{\text{AP}}^{\text{RIS}})}^\perp \mathbf{\Gamma}) \right\}, \quad (17)$$

where $\mathbf{\Gamma} \in \mathbb{C}^{M \times N_{\text{epoch}}}$ is a random matrix drawn from a standard Gaussian distribution. From equation (17), we obtain $\beta_m^{(n)}$ as

$$\beta_m^{(n)} = \left[\angle(\mathcal{P}_{\mathbf{a}_M(\theta_{\text{RIS}}^{\text{RIS}})}^\perp \mathbf{\Gamma}) \right]_{n,m}, \quad \forall n, m. \quad (18)$$

In the above, note that $\beta_m^{(n)}$ is independent of the signal structure of $s(t)$. This suggests that no apriori knowledge is required at the PR and RIS. Besides the RIS, the PR beamformers towards the RIS to listen to all AP-target-RIS-PR paths. More specifically, the PR applies a static beamforming vector \mathbf{w} as follows

$$\begin{aligned} \mathbf{w}^H \mathbf{Y}_n &= \rho_{\text{RIS}}^{\text{PR}} \mathbf{w}^H \mathbf{a}(\theta_{\text{RIS}}^{\text{PR}}) \mathbf{x}_n \\ &+ \mathbf{w}^H \left(\rho_{\text{AP}}^{\text{PR}} \mathbf{h}_{\text{AP}}^{\text{PR}} \mathbf{s}_{\text{AP}}^{\text{PR}} + \sum_{k=1}^K \rho_k \mathbf{h}_k^{\text{PR}} \mathbf{s}_k^{\text{PR}} + \mathbf{E}_n \right). \end{aligned} \quad (19)$$

over all epochs $n = 1 \dots N_{\text{epoch}}$. The first term is the signal-of-interest needed at the PR to localize the targets, whereas the second and third terms contain weak LoS signals that can not be reliably used for localization. Although a simple choice of $\mathbf{w} = \frac{\mathbf{a}(\theta_{\text{RIS}}^{\text{PR}})}{\|\mathbf{a}(\theta_{\text{RIS}}^{\text{PR}})\|^2}$ is straightforward, a significant illumination towards the RIS is attained by spatially filtering out other contributions not reflected by the RIS. After beamforming at each time epoch, the collected data are stacked as

$$\begin{aligned} \mathbf{Z} &= [\mathbf{Y}_1^H \mathbf{w} \quad \mathbf{Y}_2^H \mathbf{w} \quad \dots \quad \mathbf{Y}_{N_{\text{epoch}}}^H \mathbf{w}]^H \\ &= [\mathbf{z}_1 \quad \mathbf{z}_2 \quad \dots \quad \mathbf{z}_L], \end{aligned} \quad (20)$$

where $\mathbf{Z} \in \mathbb{C}^{N_{\text{epoch}} \times L}$ is the beamformed data matrix at the PR over all epochs and time samples. In the next section, we introduce a method for joint detection of the number of targets and target AoA estimation. The algorithm iteratively updates the steering vector to minimize the error cost function, and a peak-finding search on the computed power spectrum yields estimates for the target AoAs.

IV. TARGET DETECTION AND LOCALIZATION

In this section, we describe a NLMS approach towards simultaneous detection of number of targets and target localization. First, given a matrix \mathbf{Z} representing the data received at the PR, the objective is to estimate all angles within $\Theta_{1:K}^{\text{RIS}}$, encompassing all target Angle of Arrival (AoA) information. However, in various scenarios, particularly dynamic environments, the number of targets denoted as K may be unknown. In this context, consider the output of the sum-and-delay beamformer at a specific direction θ , utilizing the steering vector $\mathbf{V}_{\mathbf{a}_M}(\theta)$ at the ℓ^{th} snapshot, expressed as

$$p_\ell(\theta) = \mathbf{a}_M^H(\theta) \mathbf{V}^H \mathbf{z}_\ell. \quad (21)$$

Subsequently, we can formulate the error cost function that we aim to minimize in each snapshot, namely $C(\ell) = \mathbb{E}(|e(\ell)|^2)$, where $e(\ell) = p_\ell(\theta) - \mathbf{a}^H \mathbf{z}_\ell$. The least mean squares (LMS) aims at minimizing the above cost. First, we take the gradient with respect to \mathbf{a} to get

$$\nabla_{\mathbf{a}} C(\ell) = 2\mathbb{E}\{\nabla_{\mathbf{a}}[e(\ell)]e^*(\ell)\} = -2\mathbb{E}\{(p_\ell(\theta) - \mathbf{a}^H \mathbf{z}_\ell)^* \mathbf{z}_\ell\},$$

where the last step is due to the gradient's value, $\nabla_{\mathbf{a}}[e(\ell)] = -\mathbf{z}_\ell$. Thanks to $\nabla_{\mathbf{a}} C(\ell)$, the LMS filter can now focus towards the steepest ascent of $C(\ell)$ by taking a direction opposite to $\nabla_{\mathbf{a}} C(\ell)$, namely

$$\begin{aligned} \hat{\mathbf{a}}_{\ell+1}(\theta) &= \hat{\mathbf{a}}_\ell(\theta) - \frac{\mu}{2} [\nabla_{\mathbf{a}} C(\ell)]_{\mathbf{a}=\hat{\mathbf{a}}_\ell} \\ &= \hat{\mathbf{a}}_\ell(\theta) + \mu \mathbb{E}\{(p_\ell(\theta) - \hat{\mathbf{a}}_\ell^H(\theta) \mathbf{z}_\ell)^* \mathbf{z}_\ell\}, \end{aligned} \quad (22)$$

where $\frac{\mu}{2}$ is the well-known LMS adaptation constant, i.e. the step size. Now that we have an update equation for the steering vector in the θ 's look-direction, the only problem that remains is the expectation operator, which is not available at time update ℓ . Therefore, omitting it we finally have

$$\hat{\mathbf{a}}_{\ell+1}(\theta) = \hat{\mathbf{a}}_\ell(\theta) + \mu(p_\ell(\theta) - \hat{\mathbf{a}}_\ell^H(\theta) \mathbf{z}_\ell)^* \mathbf{z}_\ell. \quad (23)$$

A normalized LMS, i.e. NLMS, could also be proposed at

Algorithm 1 Batch NLMS filter Localization

```

1: INPUT  $\mathbf{Z} = [\mathbf{z}_1 \quad \dots \quad \mathbf{z}_L]$ ,  $\mu$ ,  $\Theta_{\text{grid}}$ 
2: while  $\theta \neq \emptyset$  do
3:    $\hat{\mathbf{a}}_0(\theta) \leftarrow \mathbf{0}_{N_{\text{epoch}} \times 1}$ 
4:    $\ell \leftarrow 0$ 
5:   while  $\ell < L$  do
6:      $p_\ell(\theta) \leftarrow \mathbf{a}_M^H(\theta) \mathbf{V}^H \mathbf{z}_\ell$ 
7:      $\hat{\mathbf{a}}_{\ell+1}(\theta) \leftarrow \hat{\mathbf{a}}_\ell(\theta) + \frac{\mu}{\|\mathbf{z}_\ell\|} (p_\ell(\theta) - \hat{\mathbf{a}}_\ell^H(\theta) \mathbf{z}_\ell)^* \mathbf{z}_\ell$ 
8:      $\ell \leftarrow \ell + 1$ 
9:   end while
10:   $P(\theta) = \|\hat{\mathbf{a}}_L(\theta)\|^2$ 
11:  Choose next  $\theta \in \Theta_{\text{grid}}$ 
12: end while
13: if  $P(\theta)$  is peak then
14:   Insert  $\theta$  in  $\hat{\Theta}_{1:K}^{\text{RIS}}$ 
15: end if
16: return  $\hat{\Theta}_{1:K}^{\text{RIS}}$ 

```

this point to avoid sensitivities of the input norm, i.e. $\|\mathbf{z}_\ell\|$, which makes it extremely difficult to choose an adaptation constant for algorithm stability purposes [19]. To this end, the following update is proposed

$$\hat{\mathbf{a}}_{\ell+1}(\theta) = \hat{\mathbf{a}}_\ell(\theta) + \frac{\mu}{\|\mathbf{z}_\ell\|} (p_\ell(\theta) - \hat{\mathbf{a}}_\ell^H(\theta) \mathbf{z}_\ell)^* \mathbf{z}_\ell. \quad (24)$$

As $\hat{\mathbf{a}}(\theta)$ encompasses signal contributions at direction θ , a meaningful metric would be to quantify the overall power within the estimate $\hat{\mathbf{a}}_L(\theta)$, denoted as

$$P(\theta) = \|\hat{\mathbf{a}}_L(\theta)\|^2. \quad (25)$$

Ultimately, the computation of the K target AoAs is performed by conducting a one-dimensional peak-finding search on $P(\theta)$, namely

$$\hat{\Theta}_{1:K}^{\text{RIS}} = \arg \max_{\theta_1 \dots \theta_K} P(\theta). \quad (26)$$

A summary of an implementation of the proposed LMS filtering approach is summarized in **Algorithm 1**. One interesting feature of this batch approach is that it could be parallelized over angles to be evaluated on a grid, i.e. Θ_{grid} .

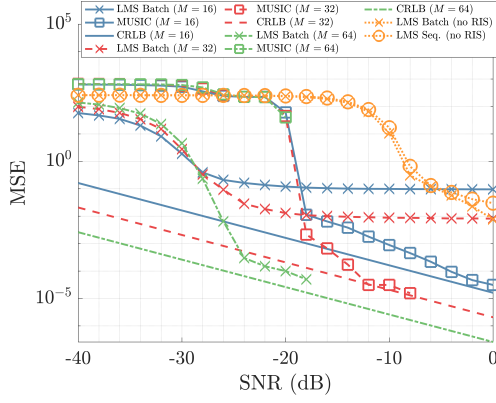


Fig. 2. The MSE vs. SNR performances of batch NLMS, sequential NLMS, MUSIC-based estimation and CRLB, with $K = 2$ targets, for ULA configuration of $N_{\text{PR}} = 8$, $L = 100$, and different values of M .

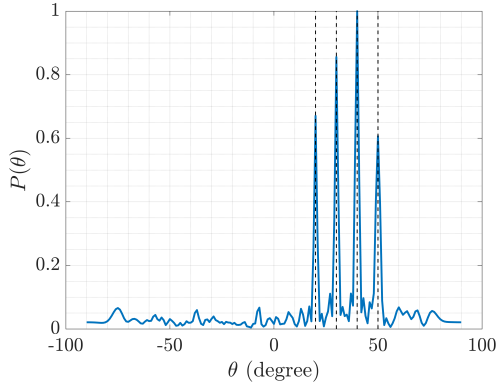


Fig. 3. The spectrum of the proposed NLMS method utilizing the RIS-aided architecture. The scene consists of $K = 4$ targets located at $\theta_k^{\text{RIS}} = 20 + 10(k - 1)$, $\forall k$. The RIS is equipped with $M = 64$ reflective elements and the number of time samples is $L = 100$. The number of epochs is set to $N_{\text{epoch}} = 100$. Dashed vertical lines represent the true AoAs.

In the process of peak detection, it is essential to normalize the entire spectrum $P(\theta)$ to ensure its maximum value is set to 1. Then, peak identification is done by selecting peaks surpassing a specified threshold value, denoted as $0 < \varphi < 1$.

V. SIMULATION RESULTS

In this section, we showcase various simulation outcomes designed to demonstrate the efficacy of the proposed approaches. Before, we introduce the parameter configuration and elucidate the benchmarks employed for the simulation. The number of time samples is set to $L = 100$. Additionally, the PR is equipped with $N_{\text{PR}} = 8$ antenna elements. The peak detection threshold, utilized in both batch and sequential NLMS method outlined in **Algorithm 1**, is set to $\varphi = 0.5$. The AoAs between the AP and the RIS, as well as the RIS and the PR, are fixed at $\theta_{\text{AP}}^{\text{RIS}} = -10^\circ$ and $\theta_{\text{RIS}}^{\text{PR}} = -40^\circ$, respectively. A ULA configuration with half-wavelength spacing is employed at the PR. Unless specified otherwise, the number of epochs is maintained at $N_{\text{epoch}} = 100$. To facilitate

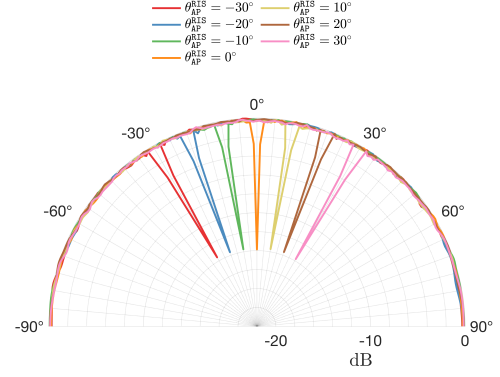


Fig. 4. Normalized RIS beampattern for different AP positions.

performance comparisons, our performance study incorporates the following benchmarks:

- **No-RIS Assistance:** In this scenario, the benchmark does not accommodate a RIS for redirecting bounces from the targets. Without the RIS, this benchmark lacks the ability to beamform towards a RIS, requiring the PR to estimate the target AoAs embedded within \mathbf{h}_k^{PR} . Therefore, the PR in this case observes

$$\mathbf{Y} = \rho_{\text{AP}}^{\text{PR}} \mathbf{h}_{\text{AP}}^{\text{PR}} \mathbf{s}_{\text{AP}}^{\text{PR}} + \sum_{k=1}^K \rho_k \mathbf{h}_k^{\text{PR}} \mathbf{s}_k^{\text{PR}} + \mathbf{E}_n. \quad (27)$$

For this benchmark, **Algorithm 1** can be repurposed. In this case, the algorithm estimates θ_k^{PR} instead of θ_k^{RIS} due to the absence of an RIS. Specifically, the input becomes \mathbf{Y} , and line 6 is replaced with $p_\ell(\theta) \leftarrow \mathbf{a}^H(\theta) \mathbf{y}_\ell$ since there is no reflective coefficient matrix \mathbf{V} . Additionally, line 7 is modified to $\hat{\mathbf{a}}_{\ell+1}(\theta) \leftarrow \hat{\mathbf{a}}_\ell(\theta) + \frac{\mu}{\|\mathbf{z}_\ell\|} (p_\ell(\theta) - \hat{\mathbf{a}}_\ell^H(\theta) \mathbf{y}_\ell) \mathbf{y}_\ell$.

- **CRLB Benchmark:** We also include the CRLB benchmark, which is not derived in this paper due to lack of space. Indeed, this benchmark aims at quantifying how good an estimator is operating as compared to the best un-biased estimator of target AoAs via the proposed RIS-aided architecture for target localization.
- **MUSIC-based Estimation with complete knowledge of number of targets:** For benchmarking, we also design a Multiple Signal Classification (MUSIC) estimator tailored for estimating target AoAs at the PR using the proposed architecture. This estimator is aware of the true number of targets in the environment, which is further used to correctly separate signal and noise subspaces.

In Fig. 2, we aim at analyzing the MSE as a function of SNR at the PR. The MSE is computed as

$$\text{MSE} = \frac{1}{PK} \sum_{k=1}^K \sum_{p=1}^P (\theta_k - \hat{\theta}_k)^2, \quad (28)$$

The parameter θ_k is the true AoA of the k^{th} target and $\hat{\theta}_k$ is the estimated AoA of the k^{th} target. We have simulated two targets, i.e. $K = 2$. Also, P is the number of Monte-carlo

trials. We aim at showing the performance for increasing number of reflective elements and for different benchmarks. First, we note that the batch NLMS method approaches the CRLB upon increasing M . Focusing on $M = 16$ elements, we also observe that at a target MSE of 0.2, the batch NLMS algorithm requires about SNR = -26 dB, whereas the MUSIC-based method requires an additional 5.75 dB compared to the NLMS algorithm. At this MSE level, a gain superior to 20 dB can be attained. Beyond -18 dB, we see that MUSIC dominates the NLMS methods, as MUSIC exploits the knowledge of the exact number of targets through proper segregation of signal and noise subspaces.

Fig. 3 shows the spectrum obtained by the proposed NLMS filtering methods. It is clear from the simulation that the peaks are sharp enough to successfully resolve the $K = 4$ targets. The low noise level is low and the detected peaks can be relied upon to detect the existence of targets at the locations, because the peak values surpass the threshold $\varphi = 0.5$.

In Fig. 4, we study the normalized beampattern at the RIS for different placements of the AP with respect to the RIS, i.e. by varying $\theta_{\text{AP}}^{\text{RIS}}$. This gives an idea regarding the DR reduction that can be attained. In this simulation, we set $N_{\text{PR}} = 16$ antennas, with $M = 64$ elements and $L = 90$ samples. In particular, we solve for the phase shifts and set the phase shifts in $\Theta^{(n)}$ as given by problem (\mathcal{P}_{RIS}), i.e. we configure $\Theta^{(n)}$ following equation (18). Next, we plot the beampattern at the RIS. Indeed, according to equation (3), the beampattern reads

$$B(\theta) = \sum_n \mathbf{a}_M^H(\theta) (\Theta^{(n)})^H \mathbf{b}_M^*(\phi_{\text{RIS}}^{\text{PR}}) \mathbf{b}_M^T(\phi_{\text{RIS}}^{\text{PR}}) \Theta^{(n)} \mathbf{a}_M(\theta).$$

The pattern suggest that for different values of $\theta_{\text{AP}}^{\text{RIS}}$, the RIS is successfully able to redirect the target bounces at around 0 dB (quasi-distortionless), while attenuating the channel between the AP and itself by about 14 dB. This means that the analog-to-digital converter (ADC) at the PR can operate with a reduced DR of 14 dB.

VI. CONCLUSIONS AND FUTURE WORK

In short, this paper addresses the challenges faced by PR in scenarios with weak LoS signals, particularly those caused by communication signals from an AP and further reflected off targets. The deployment of RIS with strong LoS coverage between itself and the AP, as well as the PR, is proposed to overcome the limitations of weak LoS signals. The key contributions of this work include the formulation of a comprehensive system model, the introduction of a collaborative RIS-PR beamforming strategy to enhance LoS signal reception for localization, while keeping a reasonably low DR at the PR for ADC power consumption purposes, and the presentation of an adaptive approach based on NLMS for joint target number detection and AoA estimation. Simulation results showcase the effectiveness of the proposed method, highlighting a significant 14 dB reduction in DR achievable at the PR. This research offers valuable insights into improving the performance of PR systems in challenging communication environments. Future work will focus on designing and solving

optimization frameworks that can achieve a lower DR, while maintaining a good localization and detection performance.

REFERENCES

- [1] M. D. Renzo, M. Debbah, D.-T. Phan-Huy, A. Zappone, M.-S. Alouini, C. Yuen, V. Sciancalepore, G. C. Alexandropoulos, J. Hoydis, H. Gacanin *et al.*, "Smart radio environments empowered by reconfigurable AI meta-surfaces: An idea whose time has come," *EURASIP Journal on Wireless Communications and Networking*, vol. 2019, no. 1, pp. 1–20, 2019.
- [2] Y. Han, S. Jin, C.-K. Wen, and T. Q. Quek, "Localization and Channel Reconstruction for Extra Large RIS-Assisted Massive MIMO Systems," *IEEE Journal of Selected Topics in Signal Processing*, 2022.
- [3] S. Lin *et al.*, "Reconfigurable intelligent surfaces with reflection pattern modulation: Beamforming design and performance analysis," *IEEE Transactions on Wireless Communications*, vol. 20, no. 2, pp. 741–754, 2020.
- [4] W. Xu, J. Zhang, S. Cai, J. Wang, and Y. Wu, "RIS-assisted MIMO secure communications with Bob's statistical CSI and without Eve's CSI," *Digital Communications and Networks*, 2022.
- [5] G. Zhou, C. Pan, H. Ren, P. Popovski, and A. L. Swindlehurst, "Channel estimation for RIS-aided multiuser millimeter-wave systems," *IEEE Transactions on Signal Processing*, vol. 70, pp. 1478–1492, 2022.
- [6] C. Huang, A. Zappone, G. C. Alexandropoulos, M. Debbah, and C. Yuen, "Reconfigurable intelligent surfaces for energy efficiency in wireless communication," *IEEE Transactions on Wireless Communications*, vol. 18, no. 8, pp. 4157–4170, 2019.
- [7] C. Liaskos, A. Tsioliaridou, A. Pitsillides, S. Ioannidis, and I. Akyildiz, "Using any surface to realize a new paradigm for wireless communications," *Communications of the ACM*, vol. 61, no. 11, pp. 30–33, 2018.
- [8] B. Dawidowicz, P. Samczynski, M. Malanowski, J. Misiurewicz, and K. Kulpa, "Detection of moving targets with multichannel airborne passive radar," *IEEE Aerospace and Electronic Systems Magazine*, vol. 27, no. 11, pp. 42–49, 2012.
- [9] E. C. Strinati, G. C. Alexandropoulos, V. Sciancalepore, M. Di Renzo, H. Wymeersch, D.-T. Phan-Huy, M. Crozzoli, R. d'Errico, E. De Carvalho, P. Popovski *et al.*, "Wireless environment as a service enabled by reconfigurable intelligent surfaces: The RISE-6G perspective," in *2021 Joint European Conference on Networks and Communications & 6G Summit (EuCNC/6G Summit)*. IEEE, 2021, pp. 562–567.
- [10] A. Bazzi and M. Chafii, "On Integrated Sensing and Communication Waveforms With Tunable PAPR," *IEEE Transactions on Wireless Communications*, vol. 22, no. 11, pp. 7345–7360, 2023.
- [11] A. Taha, M. Alrabeiah, and A. Alkhateeb, "Enabling large intelligent surfaces with compressive sensing and deep learning," *IEEE access*, vol. 9, pp. 44 304–44 321, 2021.
- [12] J. He, H. Wymeersch, T. Sanguanpuak, O. Silven, and M. Juntti, "Adaptive Beamforming Design for mmWave RIS-Aided Joint Localization and Communication," in *2020 IEEE Wireless Communications and Networking Conference Workshops (WCNCW)*, 2020, pp. 1–6.
- [13] A. Fascista, A. Coluccia, H. Wymeersch, and G. Seco-Granados, "RIS-aided joint localization and synchronization with a single-antenna mmwave receiver," in *ICASSP 2021-2021 IEEE International Conference on Acoustics, Speech and Signal Processing (ICASSP)*. IEEE, 2021, pp. 4455–4459.
- [14] A. Elzanaty, A. Guerra, F. Guidi, and M.-S. Alouini, "Reconfigurable intelligent surfaces for localization: Position and orientation error bounds," *IEEE Transactions on Signal Processing*, vol. 69, pp. 5386–5402, 2021.
- [15] H. Zhang, H. Zhang, B. Di, K. Bian, Z. Han, and L. Song, "Metalocalization: Reconfigurable intelligent surface aided multi-user wireless indoor localization," *IEEE Transactions on Wireless Communications*, vol. 20, no. 12, pp. 7743–7757, 2021.
- [16] Z. He, Y. Yang, W. Chen, and D. Weng, "Range Resolution Improvement of GNSS-Based Passive Radar via Incremental Wiener Filter," *IEEE Geoscience and Remote Sensing Letters*, vol. 19, pp. 1–5, 2022.
- [17] Z. Esmailbeig, A. Eamaz, K. V. Mishra, and M. Soltanalian, "Joint Waveform and Passive Beamformer Design in Multi-IRS-Aided Radar," in *ICASSP 2023 - 2023 IEEE International Conference on Acoustics, Speech and Signal Processing (ICASSP)*, 2023, pp. 1–5.
- [18] A. Chowdary, A. Bazzi, and M. Chafii, "On Hybrid Radar Fusion for Integrated Sensing and Communication," *IEEE Transactions on Wireless Communications*, pp. 1–1, 2024.
- [19] S. Haykin, "Adaptive filter theory 3rd edition Prentice-Hall," 1996.